

The Utilization of Image Subtraction and Wavelet Decomposition-Reconstruction for Improving FCM Based Segmentation of Radiographic Weld Defect

Muhtadan

Polytechnic Institute of Nuclear Technology-National Nuclear Energy Agency
Jl. Babarsari P.O. Box 6101 YKBB 55281 Yogyakarta, Indonesia

Copyright © 2015 Muhtadan. This article is distributed under the Creative Commons Attribution License, which permits unrestricted use, distribution, and reproduction in any medium, provided the original work is properly cited.

Abstract

Automatic weld defect segmentation is an important step in radiographic weld defect identification system. Fuzzy C Means (FCM) clustering, which had been proven capable and applied for many images segmentation applications, was utilized as the segmentation basis of weld defect object. In this study, a method using Laplacian sharpening of image subtraction and 2-D wavelet decomposition-reconstruction is utilized for improving the result of FCM-based weld defect segmentation. Image subtraction was applied by subtracting the background image, which was estimated by 30×60 average filtering, with the origin image and followed by image sharpening operation using Laplacian filtering to reduce the background intensity and to enhance the foreground area. Two level decomposition of 2D db4 wavelet was employed to produce wavelet coefficients, then 2 levels wavelet reconstruction was performed only using approximation coefficient to synthesize a new image. In the last step, reconstructed image was segmented by FCM clustering to obtain a weld defect image. The proposed method was tested on five different weld defect types sample and it was evaluated using mutual overlap approach. The evaluation result showed that this method increase the mutual overlap metric which obtained 57.46%.

Keywords: Radiographic weld defect segmentation, fuzzy c means, image subtraction, wavelet decomposition-reconstruction

1 Introduction

Industrial radiography is applied for evaluating and detecting metal weld defect or material casting discontinuity. Radiography utilizes high activity photon, either from radioisotope-excited gamma ray or from an x-ray generator. Radiograph that produced by this technique give information about the welding structure, including its defect or discontinuity i.e. crack, porosity, slag inclusion, and lack of penetration [1]. Computer aided based radiograph analysis has being developed by many researcher to reduce the disadvantage of the conventional method. An important issue on this system for image analysis is the segmentation. The aim of radiograph image segmentation is to separate the weld defect region from other object regions on the radiograph image like base material, weld area, and another object. Due to radiograph image quality is worse, which it has low contrast, low signal to noise ratio, and another object that has high weld defect similarity, then it places the image segmentation as important problem to be performed in computer aided radiograph identification system.

Various works of weld defect segmentation have being developed by many researchers using many methods and approaches. Here is the summary of several previous works in the weld defect segmentation. Thresholding technique was applied for separating weld defect region based on its intensity characteristic. There are two model of thresholding that based on determination area of threshold value. First model is local thresholding that determine the threshold value from several technique i.e the intensity of image pixel on specific area [2, 3], average of intensity value [4], and multiple threshold by iterating specific window [5]. The second model is global thresholding or Otsu thresholding [6] that determine threshold value from the intensity value of the whole image area or pixels.

Background subtraction is an alternative method for separating weld defect object area. Principally, this method subtracts an image by other image as its background image. Background image can be estimated using several methods i.e surface fitting algorithm and polynomial function [7], low-pass filter on the origin image using 30×60 sized average filter [8]. Generally, segmentation based on background subtraction utilization produces good segmented weld defect region, however this method is weak for detecting weld defect region that smaller than estimation function output value or filter size, because the smaller regions will be eliminated by either estimation function or filter size.

An automatic weld defect segmentation can be developed using unsupervised classification or clustering method. Fuzzy C Means (FCM) is one of clustering method that has been proven and applied in other image segmentation applications. In application of weld defect detection, FCM has been utilized for isolating area that contain defects, and then weld defect was detected by improved thresholding method [9]. However, the utilization of FCM in their work was not used yet for weld defect segmentation and their method was not tested for other weld defect types. In this study, a Laplacian filter based sharpening of image subtraction and two level decomposition-reconstruction of 2-D wavelet were utilized

to improve the FCM based segmentation of radiographic weld defect. The results of this segmentation method were tested and evaluated using five different weld defect types. In the end of discussion, the quantitative results of segmentation evaluation were also compared with the basic FCM segmentation method.

2 Methods

In this study, radiographic weld defect segmentation was performed by utilized FCM clustering based method. This segmentation approach was improved by applied image subtraction and 2-D wavelet decomposition-reconstruction to obtained segmented image, which contains weld defect object that separated from other non-defect object or noise.

Radiographic film is divided to be several areas for weld defect segmentation purpose i.e material base area, weld area, and weld defect object area [10]. This study focused only in the weld defect object segmentation. The experimental procedures of weld defect object segmentation are shown in Fig. 1.

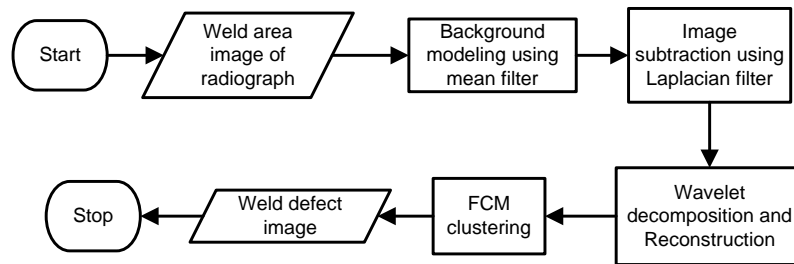


Fig. 1. The procedures of weld defect object segmentation

The weld area image of radiograph was determined by determining the region of interest (ROI) of digital radiograph. The ROI is utilized to eliminate the material based area from weld area and weld defect object area. The weld area image was used in background modelling and image subtraction as the first step. The principal of image subtraction is to subtract image with its background, so that obtained high intensity foreground images. In this study, the background image was obtained by carrying out a filtering operation using 30×60 average filter as performed by [8]. Then, the procedure was performed by applied Laplacian image sharpening to enhance the foreground of subtracted image. The Laplacian image $\nabla^2 f(x, y)$ was obtained by calculated every pixel using Eq. (1), where $f(x, y)$ was an intensity image on x and y axis, and w was a Laplacian filter kernel that calculated using Eq. (2) and by determining the α value [11].

$$\nabla^2 f(x, y) = \sum (w \cdot f(x, y)) \quad (1)$$

$$w = \frac{4}{\alpha + 1} \begin{bmatrix} \frac{\alpha}{4} & \frac{1-\alpha}{4} & \frac{\alpha}{4} \\ \frac{1-\alpha}{4} & -1 & \frac{1-\alpha}{4} \\ \frac{\alpha}{4} & \frac{1-\alpha}{4} & \frac{\alpha}{4} \end{bmatrix} \quad (2)$$

The sharpened image was obtained by subtracting $f(x,y)$ with $\nabla^2 f(x,y)$. Let an image f was an origin image, here was the procedure of the Laplacian image subtraction.

1. Create the 30×60 sized average filter w_1 .
2. Perform image filtering of image f using w_1 to obtain background image g_1 .
3. Subtract g_1 by f to obtain subtracted image f_1 .
4. Create Laplacian filter w_2 using Eq. (2).
5. Create Laplacian image g_2 by applied filtering of f with w_2 using Eq. (1).
6. Subtract f_1 by g_2 to obtain the sharpened of subtracted image f_2 .

The 1st-3rd step was used for eliminated background image and noise, while the rest step employed the second derivative operation for increased foreground intensity.

The second step was 2-D wavelet decomposition and reconstruction. Image wavelet decomposition is an image analysis process to yield wavelet coefficients. Wavelet reconstruction is synthesis process or inverse transformation of decomposition. Fig 2 is called as single scale filter bank or 1 scale (1 level) wavelet decomposition. These processes can be iterated by connected approximation output $W\varphi(j, m, n)$ in another filter bank input to give result of P -scale decomposition, which $j = J-1, J-2, \dots, J-P$.

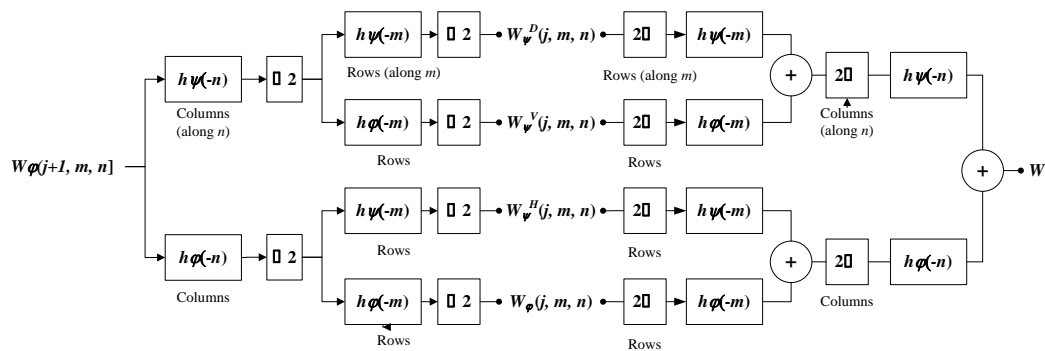


Fig. 2. Single scale filter bank for wavelet decomposition and reconstruction

In this study, 2D wavelet decomposition-reconstruction was used to obtain reconstructed image using only its approximation coefficient. This process was performed by carrying out these steps:

1. Select a wavelet mother and determine the number of P -scale decomposition.
2. Perform P level wavelet transformation, then obtained P level wavelet coefficients.

3. Change all detail coefficient values $W\psi^H(j, m, n)$, $W\psi^V(j, m, n)$, and $W\psi^D(j, m, n)$ to zero.
4. Use all coefficients to performed reconstruction process to obtain a synthesized image.

The last step was FCM segmentation. FCM is an unsupervised classification method that parting data into two or more classes by consider that all samples have probability as a member in each class. In this study, FCM based segmentation of image size $[M, N]$ was done by performed the following steps:

1. Reshape the image from $[M, N]$ matrix form into $[MN, 1]$ matrix form.
2. Determine the value of $c = 3$, $q = 2$, $\varepsilon = 10^{-6}$, and maximum iteration = 200
3. Initialize $[c, MN]$ sized $U^{(t)}$ matrix randomly. Each i sample should be met with $\sum_{j=1}^c u_{ij} = 1$. The first t value was 0.
4. Calculate v_i using Eq. 3 [12] and $U^{(t)}$, then calculate $J^{(t)}(U, v)$ using Eq. 4 [12].

$$v_i = \frac{\sum_{j=1}^n (u_{ij})^q x_j}{\sum_{j=1}^n (u_{ij})^q} \quad (3)$$

$$J(U, v) = \sum_{i=1}^c \sum_{j=1}^n u_{ij}^q \|x_j - v_i\|^2 \quad (4)$$

$$u_{ij} = \frac{1}{\left(\sum_{k=1}^c \frac{\|x_j - v_k\|^{2/(q-1)}}{\|x_j - v_k\|^{2/(q-1)}} \right)} \quad (5)$$

5. Calculate $U^{(t)}$ matrix using Eq. 5 [12].
6. Calculate $\Delta J = J^{(t+1)}(U, v) - J^{(t)}(U, v)$.
7. Repeat step 4 to 7 until $\Delta J \leq \varepsilon$ or $t =$ maximum iteration.

The output of FCM clustering, which it was $[c, MN]$ sized matrix, would be used to obtain c labeled images as images of segmentation result. This result was obtained by performed the following steps:

1. Create vector y that its elements were c values, where $u(c)$ in each element of U matrix was maximum.
2. Reshape the $[1, MN]$ sized vector y into $[M, N]$ sized matrix g .
3. Count the number of pixel in each label of the image g from its histogram, then determine the label l , which it had smaller pixel number.
4. Set all l labeled pixel value in the image g into 1, and other pixels were 0.

The label with smaller pixel number was decided as weld defect, because the area of weld defect generally was smaller than other area in radiographic image.

3 Result and discussion

The ROI image was used as image input for weld defect object segmentation. The radiograph sample and its ROI image result is shown in Fig. 3. In the image subtraction stage, the result of estimated background image from Fig. 3b is shown in Fig. 4a.



Fig 3. (a) the digital image of radiograph, and (b) its ROI image result.

The subtraction of image and its estimated background gives the image result that its intensity has more higher than its background but there is still another background or noise intensity, so that the Laplacian image sharpening was employed to reduce the noise and produces an sharpened image that is shown in Fig. 4b.

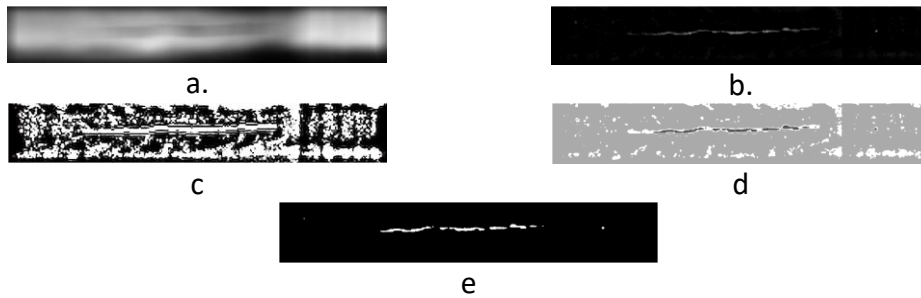


Fig. 4. Images result, (a) background modelling, (b) Laplacian subtraction, (c) 2D wavelet decomposition and resolution result, (d) three classes FCM clustering, and (e) thresholding result as segmented image.

In the wavelet decomposition-reconstruction stages, the 4th order Daubechies wavelet (*db4*) and 2 levels of decomposition-reconstruction were used. The result of 2D wavelet decomposition and reconstruction image is shown in Fig 4c. FCM clustering classifies the reconstructed image into 3 classes of intensity by applying the clustering procedures that have been described in previous section. The result of FCM clustering that is shown in Fig 4d has three values of intensity *i.e.* 85, 170, and 255. In order to get the weld defect object intensity, the thresholding was employed to found the intensity that has the fewest pixel number, because in a radiographic film, the weld defect regions is fewest than the other regions. This thresholding result is a binary image of weld defect that is shown in Fig 4e.

The method of segmentation in this study is also tested on other different weld defect type, *i.e.* crack, porosity, burn trough, and slag inclusion. Then a mutual overlap approach was employed to evaluate the segmentation result quantitatively.

The objective of this approach is to measure the mutual overlap metric between ground truth image (A_1) and the segmentation image (A_2). The ground truth image is obtained by determining the weld defect object manually based on radiographic expert decision. Then, evaluation metric is known by calculating the mutual overlap metric (M_{MO}) as is formulated by [13] that is shown in Eq. 6

$$M_{MO} = \frac{2MO}{A_1 + A_2} \quad (6)$$

Table 1 shows the comparison of M_{MO} between Otsu's thresholding, ordinary FCM, and the proposed method for different weld defect type. The M_{MO} average of ordinary FCM is 0.0213 and the M_{MO} average of the proposed method is 0.5958. This means that the using of image subtraction and wavelet decomposition-reconstruction can improve the result of FCM based segmentation until 57.46%.

Table 1. Mutual overlap metric comparison of several segmentation method

Weld defect type	Otsu's thresholding	FCM	This method
Burn trough	0.0000	0.0000	0.7012
Porosity	0.0305	0.0218	0.4522
Slag inclusion	0.0059	0.0018	0.6909
Crack	0.0083	0.0763	0.7162
Wormholes	0.0343	0.0065	0.4187

4 Conclusion

Automatic weld defect segmentation is an important stage on weld defect identification systems. This study proposes a method for improving FCM based segmentation of weld defect. This segmentation was improved by utilized an image subtraction that was modified by employed a Laplacian image sharpening, and two level decomposition-reconstructions of 2-D 4th order Daubechies wavelet. The proposed method was tested using five different weld defect types, and it was evaluated using mutual overlap approach. The evaluation result showed that this proposed method could increase the FCM segmentation result, which it was shown by its mutual overlap metric that increased until 57.46%.

References

- [1] E. M. A. Hussein, *Handbook on Radiation Probing, Gauging, Imaging and Analysis, Volume II: Applications and Design*, Kluwer Academic Publisher, 2003. <https://doi.org/10.1007/0-306-48403-x>
- [2] S. M. Alghalandis and G. N. Alamdari, "Welding defect pattern recognition

- in radiographic images of gas pipelines using adaptive feature extraction method and neural network classifier, *23rd World Gas Conference, Amsterdam, 2006*.
- [3] A. Mahmoudi and F. Regragui, Fast segmentation method for defects detection in radiographic images of welds, *2009. AICCSA 2009. IEEE/ACS International Conference on Computer Systems and Applications*, (2009), 857-860. <https://doi.org/10.1109/aiccsa.2009.5069430>
- [4] D.-H. Shi, T. Gang, S.-Y. Yang, and Y. Yuan, "Research on segmentation and distribution features of small defects in precision weldments with complex structure, *NDT & E International*, **40** (2007), 397-404. <https://doi.org/10.1016/j.ndteint.2007.01.004>
- [5] Y. Wang, Y. Sun, P. Lv and H. Wang, Detection of line weld defects based on multiple thresholds and support vector machine, *NDT&E International*, **41** (2008), 517–524. <https://doi.org/10.1016/j.ndteint.2008.05.004>
- [6] J. Zapata, R. Vilar and R. Ruiz, Performance evaluation of an automatic inspection system of weld defects in radiographic images based on neuro-classifiers, *Expert Systems with Applications*, **38** (2011), 8812-8824. <https://doi.org/10.1016/j.eswa.2011.01.092>
- [7] G. Wang and T. W. Liao, Automatic identification of different types of welding defects in radiographic images, *NDT&E International*, **35** (2002), 519–528. [https://doi.org/10.1016/s0963-8695\(02\)00025-7](https://doi.org/10.1016/s0963-8695(02)00025-7)
- [8] V. Kaftandjian, O. Dupuis, D. Babot, and Y. Min Zhu, Uncertainty modelling using Dempster–Shafer theory for improving detection of weld defects, *Pattern Recognition Letters*, **24** (2003), 547-564. [https://doi.org/10.1016/s0167-8655\(02\)00276-3](https://doi.org/10.1016/s0167-8655(02)00276-3)
- [9] H. Yazid, H. Arof, H. Yazid, S. Ahmad, A. A. Mohamed and F. Ahmad, Discontinuities detection in welded joints based on inverse surface thresholding, *NDT & E International*, **44** (2011), 563-570. <https://doi.org/10.1016/j.ndteint.2011.06.002>
- [10] T. W. Liao and J. Ni, An automated radiographic NDT system for weld inspection: Part I — Weld extraction, *NDT & E International*, **29** (1996), 157-162. [https://doi.org/10.1016/0963-8695\(96\)00009-6](https://doi.org/10.1016/0963-8695(96)00009-6)
- [11] R. C. Gonzalez and R. E. Woods, *Digital Image Processing Third Edition*, Pearson Prentice Hall, 2010.
- [12] S. R. Kannan, S. Ramathilagam, R. Devi and A. Sathya, Robust kernel FCM

in segmentation of breast medical images, *Expert Systems with Applications*, **38** (2011), 4382-4389. <https://doi.org/10.1016/j.eswa.2010.09.107>

- [13] M. Sonka, V. Hlavac and R. Boyle, *Image Processing, Analysis, and Machine Vision*, Thomson Learning, 2008.

Received: November 1, 2015; Published: November 21, 2016